INTERNATIONAL JOURNAL FOR NUMERICAL METHODS IN ENGINEERING
Int. J. Numer. Meth. Engng 2010; **00**:1–6 *Prepared using* nmeauth.cls *[Version: 2002/09/18 v2.02]*

On the effect of the bulk tangent matrix in partitioned solution schemes for nearly incompressible fluids

Alessandro Franci[1]*, Eugenio Oñate[1,2], Josep Maria Carbonell[1,2]

[1] *Centre Internacional de Mètodes Numèrics en Enginyeria (CIMNE)*
Campus Norte UPC, 08034 Barcelona, Spain
Email: falessandro,onate@cimne.upc.edu
[2] *Universitat Politècnica de Catalunya (UPC), Email: cpuigbo@cimne.upc.edu*

SUMMARY

The purpose of this paper is to study the effect of the bulk modulus in the iterative matrix for the analysis of quasi-incompressible free surface fluid flows using a mixed Lagrangian finite element formulation and a partitioned solution scheme. A practical rule to set up the value of a pseudo-bulk modulus a priori in the tangent bulk stiffness matrix for improving the conditioning of the linear system of algebraic equations is also given. The efficiency of the proposed strategy is tested in several problems analyzing the advantage of the modified bulk tangent matrix with regard to the stability of the pressure field, the convergence rate and the computational speed of the analyses. The technique has been tested on the FIC/PFEM Lagrangian formulation presented in [19] but it can be easily extended to other quasi-incompressible stabilized finite element formulations.

KEY WORDS: Quasi-incompressible fluid, bulk modulus, mass conservation, ill-conditioning, finite calculus, finite element method, particle finite element method, partitioned scheme.

1. Introduction

Various approaches have been developed in the last years for approximating fluid flows by means of a quasi-incompressible material. In practice, they all consider the Navier-Stokes problem with a modified mass conservation equation where a slight compressibility is added to the fluid.

In previous works, see for example [7, 24, 30, 34], the fluid compressibility was introduced by relaxing the incompressibility contraint by means of a penalty parameter α in the following manner:

$$\varepsilon_v = \frac{1}{\alpha} p \tag{1}$$

*Correspondence to: CIMNE, Edificio C1, Campus Norte, UPC, Gran Capitán s/n, 08034 Barcelona, Spain

Contract/grant sponsor: Publishing Arts Research Council; contract/grant number: 98–1846389

Received 17 January 2007
Revised

where ε_v is the volumetric strain rate and p is the pressure (assumed to be positive in tension). The classical mass conservation equation for a fully incompressible fluid can be recovered from Eq.(1) by considering $\alpha \to \infty$.

Alternatively, the small compressibility in the fluid can be introduced by considering the actual bulk modulus of the fluid κ, which gives this operation a physical meaning, [8, 13, 34]. The mass conservation equation is now written as:

$$\varepsilon_v = \frac{1}{\kappa}\frac{\partial p}{\partial t} \tag{2}$$

where $\kappa = \rho c^2$, being ρ the density and c the speed of sound in the fluid. In this work, the latter approach is followed.

The success of quasi-incompressible formulations in fluid mechanics relies on their important advantages from the numerical point of view. The most obvious one is that both Eq.(1) and Eq.(2) give a direct relation between the two unknown fields of the Navier-Stokes problem, the velocities and the pressure. This is extremely useful if the problem is solved using a partitioned scheme because the velocity-pressure relation is crucial for deriving the tangent matrix of the momentum equations. Furthermore, another important drawback of the fully incompressible schemes is eluded. In fact, the incompressibility constraint leads to a diagonal block of a zero matrix in the global matrix system. Consequently, a pivoting procedure is required to solve numerically this kind of linear system. It is well known that the computational cost associated to this operation is high and it increases with the number of degrees of freedom of the problem. The compressibility terms that emanate from Eqs.(1) or (2) fill the diagonal of the global matrix overcoming these numerical difficulties.

On the other hand, quasi-incompressible schemes insert in the numerical model parameters that have typically high values and can lead to different numerical instabilities. For example, large values of the penalty parameter or, equally, physical values of the bulk modulus, can compromise the quality of the analyses or even prevent the convergence of the solution scheme, [34]. For this reason, generally, the value of the actual bulk modulus is reduced arbitrarily to the so-called *pseudo bulk modulus*. Nevertheless, an excessively small value of the pseudo bulk modulus changes drastically the meaning of the continuity equation of the original Navier-Stokes problem; in other words, the incompressibility constraint would not be satisfied at all. Furthermore, the bulk modulus is proportional to the speed of sound propagating through the material. Hence, it has to be guaranteed that the order of magnitude of the velocities of the problem is several times smaller than the velocity of sound in the medium.

In this paper, we present a new numerical solution scheme for nearly incompressible fluids that has excellent convergence and mass preservation features.

The method is based on using a pseudo-bulk modulus κ_p in the tangent matrix used for the iterative solution of the discretized momentum equations written in a Lagrangian form (using for instance the finite element method (FEM) [34]), while the actual physical value of the bulk modulus κ is used for the numerical solution of the mass conservation equation.

The pseudo-bulk modulus κ_p is defined "a priori" as a proportion of the actual bulk modulus of the fluid (i.e. $\kappa_p = \theta\kappa$ with $0 < \theta < 1$). A simple procedure for computing the scaling factor θ is presented.

The method proposed in this work is an improvement in terms of mass conservation and overall efficiency of the numerical solution scheme versus other similar methods that use an arbitrarily defined pseudo-bulk modulus in both the continuity and the mass conservation

equations [26–29].

The method presented can be also related to the so-called Augmented Lagrangian (AL) procedures for solving the Navier-Stokes equation for incompressible [2, 3, 9, 10, 32] and weakly compressible [4, 31] flows. A key problem in AL procedures is the definition of the AL parameter used for modifying the original set of momentum equations and defining the adequate preconditioning matrix.

In the method here proposed the pseudo-bulk modulus plays the role of the AL parameter in the momentum equations. On the other hand, the "compressible" form of the mass conservation matrix is used together with an adequate stabilization procedure based on the Finite Calculus (FIC) technique [16, 17, 23, 25]. The FIC stabilization method ensures the correctness of the solution for quasi and fully incompressible situations when equal order interpolation is used for the velocities and the pressure, as it is the case in this work where a linear interpolation is used for all variables.

Indeed the procedure for computing the pseudo-bulk modulus in this work can be applied for estimating the AL parameter for nearly incompressible fluids.

The method has been tested on the analysis of quasi-incompressible fluids using the stabilized Lagrangian FIC-FEM formulation presented in [19]. In the mentioned work, a particular class of Lagrangian FEM termed the Particle Finite Element Method (PFEM, www.cimne.com/pfem) [6, 14, 15, 22] is used. The PFEM treats the mesh nodes as particles which can freely move and even separate from the main fluid domain representing, for instance, the effect of water drops. A mesh connects the nodes discretizing the domain where the governing equations are solved using a stabilized FEM. A linear interpolation is adopted for both the pressure and velocity fields. This choice does not fullfil the so-called *LBB inf − sup condition* [5, 8, 33]. As mentioned above, the required stabilization is provided by the Finite Calculus (FIC) method [16, 17, 23, 25].

The lay-out of the paper is the following. In the first section the governing equations for quasi-incompressible Lagrangian fluids are given. The fully discretized form is derived using finite elements for space and a Newmark scheme for time. Then the FIC-stabilized form [19] of the problem is introduced into the numerical model. After that, the incremental solution of the discretized equations is derived. Once the formulation has been described, the effect of the bulk modulus on the solution scheme is studied. In particular, its effect on the linear solver convergence, the quality of the solution of the pressure field, the rate of convergence of the scheme and the mass conservation of the fluid are analyzed. An efficient method to predict the optimum value of the pseudo bulk modulus is then proposed. The particularization for fully incomprensible fluids is briefly described. In the last part of the paper some numerical results for water flows obtained with the method proposed are shown. The good properties of the numerical scheme in terms of general accuracy and computational efficiency are discussed.

2. Lagrangian formulation for quasi-incompressible fluids

2.1. Governing equations and fully discretized form

The governing equations of the problem are the linear momentum balance equations and the mass conservation equation for a quasi-incompressible fluid. In the Lagrangian description, the equations read:

Linear momentum balance equations

$$\rho\frac{Dv_i}{Dt} - \frac{\partial \sigma_{ij}}{\partial x_j} - b_i = 0 \quad , \quad i,j = 1, n_s \qquad in\ \Omega_t \times (0,T) \tag{3}$$

where v_i and b_i are the velocity and body force components along the ith Cartesian axis, ρ is the density of the fluid, n_s is the number of space dimensions (i.e. $n_s = 3$ for 3D problems) and σ_{ij} are the components of the Cauchy stress tensor.

Mass conservation equation

$$\varepsilon_v - \frac{1}{\kappa}\frac{\partial p}{\partial t} = 0 \quad , \qquad in\ \Omega_t \times (0,T) \tag{4}$$

where ε_v is the volumetric strain rate and κ is the bulk modulus of the fluid.

Boundary conditions

$$v_i - v_i^p = 0 \qquad \text{on } \Gamma_v \tag{5a}$$

$$\sigma_{ij} n_j - t_i^p = 0 \qquad \text{on } \Gamma_t \tag{5b}$$

where v_i^p and t_i^p, $i = 1, n_s$ are the prescribed velocities and prescribed tractions on the Dirichlet (Γ_v) and Neumann (Γ_t) boundaries, respectively.

The governing equations are discretized in space using linear shape functions for both the velocity and pressure fields according to the standard Galerkin Finite Element Method (FEM) [33]. The time discretization is performed using the classical trapezoidal rule [1]. The fully discretized form of the problem reads:

$$\left(\frac{2}{\Delta t}\mathbf{M}_v + \mathbf{K}\right)\bar{\mathbf{v}}_{n+1} + \mathbf{Q}\bar{\mathbf{p}}_{n+1} = \mathbf{f}_n \tag{6a}$$

$$\frac{1}{\Delta t}\mathbf{M}_p\left(\bar{\mathbf{p}}_{n+1} - \bar{\mathbf{p}}_n\right) - \mathbf{Q}^T\bar{\mathbf{v}}_{n+1} = \mathbf{0} \tag{6b}$$

where:

$$\mathbf{f}_n = \mathbf{f}_v + \mathbf{M}_v\left(\frac{2}{\Delta t}\bar{\mathbf{v}}_n + \dot{\bar{\mathbf{v}}}_n\right) \tag{6c}$$

In the previous equations, the subindices refer to the time step when the variable is computed and the upper bar denotes the nodal values of the unknowns. For example, $\bar{\mathbf{p}}_n$ are the nodal pressures at time $t_n = n\Delta t$.

All the matrices introduced in (6) are assembled from the element contributions given in Box 1.

$$\mathbf{M}_{v_{ij}} = \int_{\Omega^e} \rho \mathbf{N}_i^T \mathbf{N}_j d\Omega \ , \ \mathbf{K}_{ij} = \int_{\Omega^e} \mathbf{B}_i^T \mathbf{D} \mathbf{B}_j d\Omega \ , \ \mathbf{Q}_{ij} = \int_{\Omega^e} \mathbf{B}_i^T \mathbf{m} N_j d\Omega$$

$$M_{p_{ij}} = \int_{\Omega^e} \frac{1}{\kappa} N_i N_j d\Omega \ , \ \mathbf{f}_{v_i} = \int_{\Omega^e} \mathbf{N}_i^T \mathbf{b} d\Omega + \int_{\Gamma_t} \mathbf{N}_i^T \mathbf{t} d\Gamma$$

with

$$\mathbf{B}_i = \begin{bmatrix} \frac{\partial N_i}{\partial x} & 0 & 0 \\ 0 & \frac{\partial N_i}{\partial y} & 0 \\ 0 & 0 & \frac{\partial N_i}{\partial z} \\ \frac{\partial N_i}{\partial y} & \frac{\partial N_i}{\partial x} & 0 \\ \frac{\partial N_i}{\partial z} & 0 & \frac{\partial N_i}{\partial x} \\ 0 & \frac{\partial N_i}{\partial z} & \frac{\partial N_i}{\partial y} \end{bmatrix} \quad \text{and} \quad \mathbf{N}_i = \begin{bmatrix} N_i & 0 & 0 \\ 0 & N_i & 0 \\ 0 & 0 & N_i \end{bmatrix}$$

where N_i are the linear shape functions

$$\mathbf{D} = \mu \begin{bmatrix} 4/3 & -2/3 & -2/3 & 0 & 0 & 0 \\ & 4/3 & -2/3 & 0 & 0 & 0 \\ & & 4/3 & 0 & 0 & 0 \\ & & & 2 & 0 & 0 \\ \text{Sym.} & & & & 2 & 0 \\ & & & & & 2 \end{bmatrix} \quad , \quad \mathbf{m} = [1,1,1,0,0,0]^T$$

where μ is the dynamic viscosity of the fluid

Box 1. Element form of the matrices and vectors in Eqs.(6)

2.2. Stabilization procedure using FIC

The interpolation orders of the velocity and pressure fields do not fullfil the so-called *LBB inf − sup condition* [5]. Consequently the numerical scheme needs to be stabilized. The required stabilization is introduced via the Finite Calculus (FIC) technique presented in [19]. In the mentioned work, a FIC-based stabilized finite element formulation for quasi-incompressible Lagrangian fluids is presented and successfully applied to the analysis of several free surface flow problems. The formulation shows excellent mass preservation properties. The details of this formulation lie outside the objective of this work and can be found in [19]. Basically, the linear momentum equations do not change while the stabilized mass conservation equation

reads:

$$\int_\Omega \frac{q}{\kappa}\frac{Dp}{Dt}d\Omega + \int_\Omega q\frac{\tau}{c^2}\frac{D^2p}{Dt^2}d\Omega - \int_\Omega q\varepsilon_v d\Omega + \int_\Omega \tau\frac{\partial q}{\partial x_i}\left(\frac{\partial}{\partial x_i}(2\mu\varepsilon_{ij}) + \frac{\partial p}{\partial x_i} + b_i\right)d\Omega - \int_{\Gamma_t} q\tau\left[\rho\frac{Dv_N}{Dt} - \frac{2}{h_N}(2\mu\varepsilon_N + p - t_N)\right]d\Gamma = 0 \tag{7}$$

where index $(\cdot)_N$ denotes the normal projection of the variables and τ is the stabilization parameter given by:

$$\tau = \left(\frac{8\mu}{h^2} + \frac{2\rho}{\delta}\right)^{-1} \tag{8}$$

where h and δ are characteristic distances in space and time, respectively. In practice, h and δ have the same order of magnitude of the element size and the time step increment, respectively [19].

The discretized form of the stabilized mass conservation equation reads:

$$\left(\frac{1}{\Delta t}\mathbf{M}_p + \frac{1}{\Delta t^2}\mathbf{M}_{pp} + \mathbf{L} + \mathbf{M}_b\right)\bar{\mathbf{p}}_{n+1} - \mathbf{Q}^T\bar{\mathbf{v}}_{n+1} = \mathbf{g}_n \tag{9}$$

where:

$$\mathbf{g}_n = \mathbf{f}_p + \frac{1}{\Delta t}\mathbf{M}_p\bar{\mathbf{p}}_n + \frac{1}{\Delta t}\mathbf{M}_{pp}\left(\frac{\bar{\mathbf{p}}_n}{\Delta t} + \dot{\bar{\mathbf{p}}}_n\right) \tag{10}$$

All the matrices and the vectors introduced by the stabilization terms are assembled from the element contributions given in Box 2.

$$M_{pp_{ij}} = \int_{\Omega^e}\frac{\tau}{c^2}N_iN_jd\Omega\ ,\ L_{ij} = \int_{\Omega^e}\tau\left(\bigtriangledown^T N_i\right)\bigtriangledown N_j d\Omega\ ,\ M_{b_{ij}} = \int_{\Gamma_t}\frac{2\tau}{h_N}N_iN_jd\Gamma$$
$$f_{p_i} = \int_{\Gamma_t}\tau N_i\left[\rho\frac{Dv_N}{Dt} - \frac{2}{h_N}(2\mu\varepsilon_N - t_N)\right]d\Gamma - \int_{\Omega^e}\tau\bigtriangledown^T N_i\boldsymbol{b}d\Omega$$

Box 2. Element form of the stabilization matrices and vectors in Eqs.(9) and (10).

2.3. Linearization of the linear momentum equations and incremental solution

The quasi-incompressible form of the mass conservation equation (2) is useful for the linearization of the linear momentum equations as it yields a direct relation between the pressure increments and the velocities. In this way, it is easy to split the unknowns and solve the global system by means of a partitioned and incremental scheme. The iterative matrix for solving the momentum residual vector can be referred to the nodal velocities only, while the nodal pressures appear in the momentum residual vector in the right hand side.

The linearized form of the momentum equations for a time step at the $(i+1)$ -th iteration reads:

$$\mathbf{H}_v^i\Delta\bar{\mathbf{v}}^{i+1} = -\bar{\mathbf{r}}_m^i \tag{11}$$

with the momentum residual vector $\bar{\mathbf{r}}_m$ and the iteration matrix $\mathbf{H}_v$ given by

$$\bar{\mathbf{r}}_m^i = \mathbf{M}_v \dot{\bar{\mathbf{v}}}^i + \mathbf{K}\bar{\mathbf{v}}^i + \mathbf{Q}\bar{\mathbf{p}}^i - \mathbf{f}_v^i \tag{12a}$$

$$\mathbf{H}_v = \mathbf{M}_t + \mathbf{K} + \mathbf{K}_v \tag{12b}$$

where $\mathbf{M}_t$ is the mass contribution to the iteration matrix that is computed as:

$$\mathbf{M}_{t_{ij}} = \int_{\Omega^e} \mathbf{N}_i^T \frac{2\rho}{\Delta t} \mathbf{N}_j d\Omega \tag{13}$$

and $\mathbf{K}_v$ is the so-called *bulk* (or *volumetric*) *matrix* computed in the following way:

$$\mathbf{K}_v = \int_{\Omega^e} \mathbf{B}^T \mathbf{m} \Delta t \kappa_p \mathbf{m}^T \mathbf{B} d\Omega \quad , \quad \text{with } \kappa_p = \theta\kappa \tag{14}$$

where κ_p is a pseudo-bulk modulus and θ is a positive number such that $0 < \theta \leq 1$. It will be shown in the next sections that this parameter has the key-role of preventing the ill-conditioning of the iteration matrix $\mathbf{H}_v$. Notice that this matrix is an approximation of the exact tangent matrix for an Updated Lagrangian scheme [18].

Concerning the notation, the upper indices denote the iteration in the convergence loop and the subindices denote the time step when the variable is computed.

Considering the time interval $[n, n+1]$ for each iteration the following steps are carried out:

Step 1. Compute the nodal velocity increments $\Delta\bar{\mathbf{v}}$

$$\mathbf{H}_v \Delta\bar{\mathbf{v}} = -\bar{\mathbf{r}}_m^i \rightarrow \Delta\bar{\mathbf{v}} \tag{15}$$

Step 2. Update the nodal velocities

$$\bar{\mathbf{v}}_{n+1}^{i+1} = \bar{\mathbf{v}}_{n+1}^i + \Delta\bar{\mathbf{v}} \tag{16}$$

Step 3. Compute the nodal pressures $\bar{\mathbf{p}}^{i+1}$

$$\mathbf{H}_p^i \bar{\mathbf{p}}_{n+1}^{i+1} = \frac{1}{\Delta t}\mathbf{M}_p \bar{\mathbf{p}}_n + \frac{1}{\Delta t^2}\mathbf{M}_{pp}(2\bar{\mathbf{p}}_n - \bar{\mathbf{p}}_{n-1}) + \mathbf{G}^T \bar{\mathbf{v}}_{n+1}^{i+1} + \bar{\mathbf{f}}_p^i \rightarrow \bar{\mathbf{p}}_{n+1}^{i+1} \tag{17}$$

with

$$\mathbf{H}_p = \frac{1}{\Delta t}\mathbf{M}_p + \frac{1}{\Delta t^2}\mathbf{M}_{pp} + \mathbf{L} + \mathbf{M}_b \tag{18}$$

Step 4. Update the nodal positions

$$\bar{\mathbf{x}}_{n+1}^{i+1} = \bar{\mathbf{x}}_{n+1}^i + \frac{1}{2}(\mathbf{v}_{n+1}^{i+1} + \mathbf{v}_n)\Delta t \tag{19}$$

Step 5. Check convergence

Verify:

$$r_v^{i+1} = \frac{\|\Delta\bar{\mathbf{v}}\|}{\|\bar{\mathbf{v}}_n\|} \leq e_v \tag{20a}$$

$$r_p^{i+1} = \frac{\|\bar{\mathbf{p}}_{n+1}^{i+1} - \bar{\mathbf{p}}_{n+1}^i\|}{\|\bar{\mathbf{p}}_n\|} \leq e_p \tag{20b}$$

where e_v and e_p are prescribed error norms for the nodal velocities and the nodal pressures, respectively. In the examples solved in this work, $e_v = e_p = 10^{-4}$ has been fixed.

If both conditions (20) are satisfied, the next time step is considered.

Further details of the solution scheme for analysis of fluid flows using PFEM can be found in [19]. Applications of the scheme to thermally-coupled flows, problems and industrial forming process are reported in [20, 21].

Remark 1. The good behavior of the FIC-FEM formulation above described in terms of accuracy and mass conservation for analysis of quasi-incompressible fluids was verified in [19]. A study of the effect of the different stabilization terms in the mass conservation feature of the formulation was also performed in [19]. In particular the relevance of the stabilization matrix $\mathbf{M}_b$, involving computations on the Neumann boundary and the time derivative of the normal velocity term in the $\mathbf{f}_p$ vector was highlighted. Also the effect of the stabilization matrix $\mathbf{M}_{pp}$ was found to be negligible in the examples analyzed.

3. Study of the effect of the physical bulk modulus in the iterative matrix

The linearized system described in the previous section suffers from numerical instabilities due to the ill-conditioning of the iteration matrix $\mathbf{H}_v$ (12b). This problem was already pointed out in previous works where similar partitioned schemes were used [26–29]. The ill-conditioning of the iterative matrix of the linear momentum equations orginates from the different orders of magnitude of its two main contributions: the mass matrix $\mathbf{M}_t$ (13) and the bulk matrix $\mathbf{K}_v$ (14) (the contribution of the viscous matrix $\mathbf{K}$ (12b) is negligible for low values of the viscosity). Typically the terms of the bulk matrix are orders of magnitude larger than those of the mass matrix.

A reliable measure of the quality of a matrix is the *condition number* [1]. For a general matrix $\mathbf{A}$, the condition number is defined as:

$$C = cond(\mathbf{A}) = \| \mathbf{A} \| \cdot \| \mathbf{A}^{-1} \| \tag{21}$$

where, in this work, $\| \mathbf{A} \|$ denotes the norm-2 of matrix $\mathbf{A}$.

The condition number C gives an indication of the accuracy of the results from the matrix inversion and the linear equation solution. Values of C close to 1 indicate a well-conditioned matrix.

The deterioration of the quality of matrix $\mathbf{H}_v$ affects directly the convergence of the iterative linear solver. In this work, the iterative $Bi-Conjugate\ Gradient$ (BCG) solver has been used and its tolerance has been fixed to 10^{-6}.

The time step increments affect highly the conditioning of the iterative matrix $\mathbf{H}_v$. In fact, $\mathbf{M}_t$ is inversely proportional to the time increment while $\mathbf{K}_v$ depends linearly on it (see Eqs.(13) and (14)). For this reason, $\mathbf{H}_v$ is well-conditioned only for a tight range of time increments.

The objective of this section is to show the drawbacks of an ill-conditioned matrix in the iterative solution scheme. For the sake of clarity, a numerical example is used to visualize and quantify these inconveniences. The problem chosen is the 2D water sloshing in a rectangular tank. The initial geometry of the problem and the finite element mesh used for the analysis are shown in Figure 1. All the data of the problem are collected in Table I.

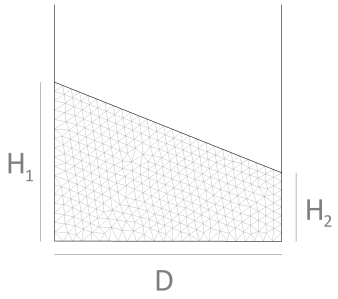

Figure 1: 2D water sloshing. Initial geometry and finite element mesh.

number of elements	705
number of nodes	428
average mesh size	0.4 m
H_1	7 m
H_2	3 m
D	10 m
viscosity	10^{-3} Pa·s
density	10^3 kg/m^3
bulk modulus	$2.15{\cdot}10^9$ Pa

Table I: 2D water sloshing. Problem data.

To highlight the importance of the time step on the conditioning of the iterative matrix, the problem has been solved for two different time increments without reducing the value of the modulus in matrix $\mathbf{K}_v$ ($\theta = 1$). Using a time step of Δt=$10^{-3}s$, the iterative matrix has a condition number C=41 while, for Δt= $10^{-2}s$, the condition number is C=3009. If a larger time step is used, the linear system can not even be solved. This deterioration is reflected by the number of iterations of the linear BCG solver: for the former case the average number of iterations is around 20, while for the latter around 177. Clearly, this also leads to a significant increase of computational time for solving a time step.

The ill-conditioning of the linear system also affects the rate of convergence of the iterative loop of the scheme given in Eqs.(15 - 20). In the graph of Fig. 2 the convergence rates 'r' for the pressure and the velocity fields at t=1.75s are displayed. These values have been obtained using Eqs.(20) and considering a time step increment of Δt=$10^{-2}s$.

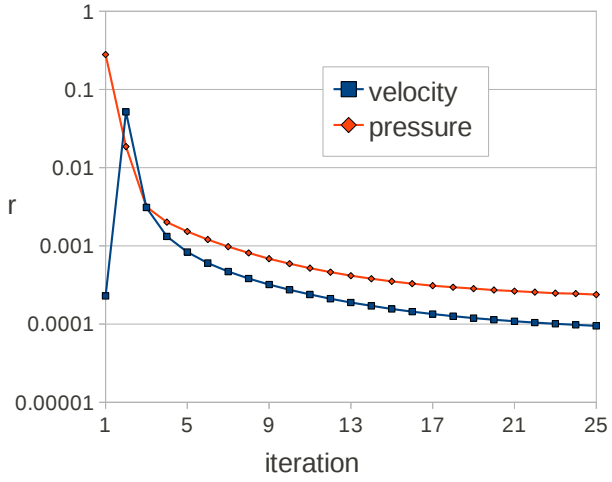

Figure 2: 2D water sloshing (θ=1). Convergence of the velocities and pressures at t=1.75 s.

It can be observed that, especially for the pressure field, the convergence criteria of Eqs.(20b) is not satisfied. In fact, the pressure error after 25 iterations is still larger than the pre-defined

tolerance of $e_p = 10^{-4}$. The lack of a good convergence for the pressure field produces two main inconveniences: the pressure solution is not accurate and mass conservation is not preserved.

The pressure contours at t=1.75 s are shown in Fig. 3.

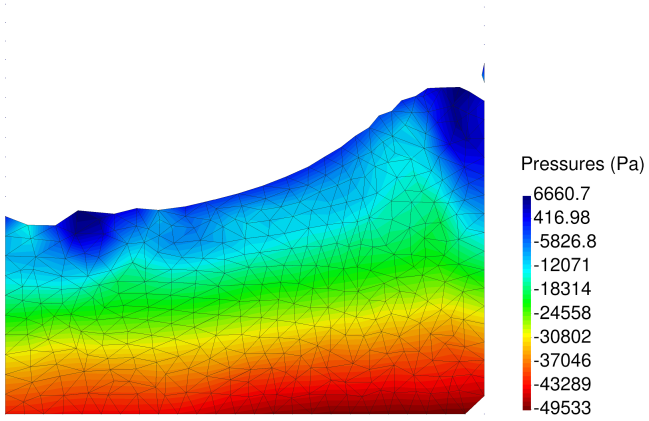

Figure 3: 2D water sloshing (θ=1). Pressure contours at t=1.75 s.

Concerning the mass conservation of the fluid, Fig. 4 shows the accumulated mass variation in absolute value versus time. After 20 seconds of simulation, the percentage of mass loss is 9.8% which corresponds to a mean volume variation of $4.9 \cdot 10^{-3}$% for each time step.

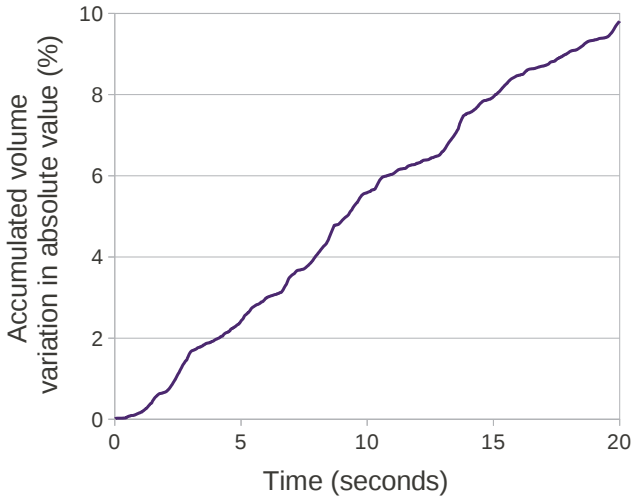

Figure 4: 2D water sloshing (θ=1). Accumulated percentage of mass variation in absolute value versus time.

4. Optimum value of the parameter θ

In the previous section it has been shown that by using $\theta = 1$ in matrix $\mathbf{K}_v$, the iteration matrix $\mathbf{H}_v$ (12b) can be ill-conditioned for certain range of time step increments. The principal consequences of this are the limitation in the choice of the time step increment and the bad convergence of both the linear iterative solver and the iterative loop described in Eqs.(15 - 20).

These inconveniences were overcome in previous publications [28, 29] by substituting the physical bulk modulus with a smaller *pseudo bulk modulus* κ_p. In this way, it is possible to extend the applicability of the partitioned scheme to a larger range of time increments. However, this strategy is based on heuristic criteria and can not be used widely because each problem requires a specific value for κ_p. In other words, a pseudo bulk modulus that works well for a certain analysis can fail for a different one.

In this section, we present a general technique for predicting *a priori* the value of the parameter θ defining the pseudo bulk modulus κ_p in Eq.(14) ($\kappa_p = \theta\kappa$). It will be shown that the strategy improves substantially the conditioning of the linear system. The enhancement is highlighted by solving the same problem of the previous section and comparing the respective results.

As pointed out in the previous sections, the numerical problem associated to the iteration matrix $\mathbf{H}_v$ (12b) is due to the different orders of magnitude of the contributions given by $\mathbf{K}_v$ (14) and $\mathbf{M}_t$ (13).

The parameter θ in Eq.(14) arises from the linearization of the pressure term in the momentum equations [19] and it can be used to scale *ad hoc* the contribution of $\mathbf{K}_v$ in order to guarantee the well-conditioning of the system. It will be shown that this operation does not interfere with the mass conservation of the fluid. The reason is that the modification only affects the quality of the iterative matrix and the rate of convergence of the linear momentum equations, while the continuity equation, where the mass conservation constraint is imposed, is not modified. This feature represents an innovation versus previous approaches where the pseudo bulk modulus is also used in the mass conservation equation.

In our work, the parameter θ is computed as:

$$\theta = \frac{mean(\mid \mathbf{M}_t \mid)}{mean(\mid \hat{\mathbf{K}}_v \mid)} \tag{22}$$

where the operator $(\mid \cdot \mid)$ denotes the mean of the absolute values of the non-zero matrix components and

$$\hat{\mathbf{K}}_v = \int_{\Omega^e} \mathbf{B}^T \mathbf{m} \Delta t \kappa \mathbf{m}^T \mathbf{B} d\Omega \tag{23}$$

The parameter θ enforces the terms contributed by $\mathbf{K}_v$ to the iteration matrix $\mathbf{H}_v$ to have the same order of magnitude as those of $\mathbf{M}_t$.

For a uniform mesh of elements of characteristic size h, θ can be estimated as follows:

$$\theta \approx \frac{2N_c^2 \cdot \rho \cdot h^2}{\kappa \cdot \Delta t^2} \tag{24}$$

where N_c is the value of the shape function N_i at the element center.

If water is considered ($\rho = 10^3 kg/m^3$ and $\kappa = 2.15 \cdot 10^9 Pa$) and linear triangles are used

($N_c = 1/3$), θ has the following dependency with the mesh size and the time step.

$$\theta \approx 10^{-7} \cdot \left(\frac{h}{\Delta t} \right)^2 \tag{25}$$

Typically, the parameter θ is calculated at the beginning of the time step at the first iteration of the non linear loop. It can also be computed at every time step, at certain instants of the analysis or only once at the beginning of the analysis. This is so because the order of magnitude of θ does not vary during the analysis, unless the time step is changed, or a refinement of the mesh is performed. In these cases, θ needs to be calculated again because it has a square dependency on both parameters h and Δt. The numerical results presented in this paper have been obtained by computing θ via Eq.(22) only at the beginning of the analyses.

The parameter θ can be computed and assigned locally to each element or globally to the whole mesh. If it is calculated globally, all the elemental bulk contributions to the iteration matrix will have the same value of θ, otherwise the computation of Eq.(22) is performed considering separately each element of the mesh; *i.e.* each element will have a different value of θ. The former approach has a reduced computational cost but it works worse than the local approach for non uniform finite element discretizations. In particular, it is recommended to use the local approach when a refinement of the mesh is performed (in the next section, a problem with a refined zone is studied). In this paper, unless otherwise mentioned, the global approach for computing θ is used.

5. Particularization for fully incompressible fluids

For fully incompressible fluids $\kappa = \infty$ and matrix $\mathbf{M}_p$ vanishes from the discretized form of the mass conservation equations (Eq.(6) and Box 1). The use of a large but finite value of the pseudo-bulk modulus κ_p in the expression of the volumetric matrix $\mathbf{K}_v$ is still useful in these cases, as it helps to obtaining an accurate solution for the velocities and the pressure with reduced mass loss in few iterations per time step. A good estimation for κ_p in these cases can be obtained as $\kappa_p = 100 \left(\frac{h}{\Delta t} \right)^2$.

6. Numerical results

The objective of the section is to assess the enhancement in the solution given by the bulk matrix scaled *a priori* by using the parameter θ computed with Eq.(22). The method is tested by solving two representative free surface problems involving the flow of water: the sloshing problem introduced in Section 3 and the collapse of a water column against a rigid obstacle presented in [12]. The so-called dam break problem has been chosen to demonstrate that the strategy does not affect the incompressibility contraint at all and the method is able to simulate problems of impact of fluids. The numerical results will be compared with the experimental ones. For both the sloshing and the dam break problems, a comparison of the performances of the scaled bulk matrix and the scheme with θ =1 is given.

In order to show the applicability and generality of the method, very different average mesh sizes and time steps are considered for both problems. It is to be noted that the dynamics of the sloshing problem is completely different from the dam break one.

6.1. Water sloshing in a tank

The problem of Fig. 1 is solved using the parameter θ computed as in Eq.(22). For Δt=$10^{-3}s$, $\theta = 0.154$, while for Δt=$10^{-2}s$, θ=0.0053. For both time step increments, the resulting condition number of the the iterative matrix is C=23 and the average number of iterations of the linear BCG solver is around 15. The improvement versus the non reduced scheme is evident, if compared with the numbers presented in Section 3. Reducing the number of iterations of the linear solver, also reduces the computational time. For example, for the problem solved with Δt=$10^{-2}s$ for a duration of $20s$, the total computational time for the case with θ=1 is $2746s$ while for θ=0.0053 it reduces to $1600s$.

Also the convergence of the non linear loop improves with the correct value of θ. In Figs. 5 and 6 the convergence of the velocity and pressure fields, respectively, obtained with θ=1 and θ=0.0053, is compared. The faster convergence of the solution using a smaller value of θ is noticeable.

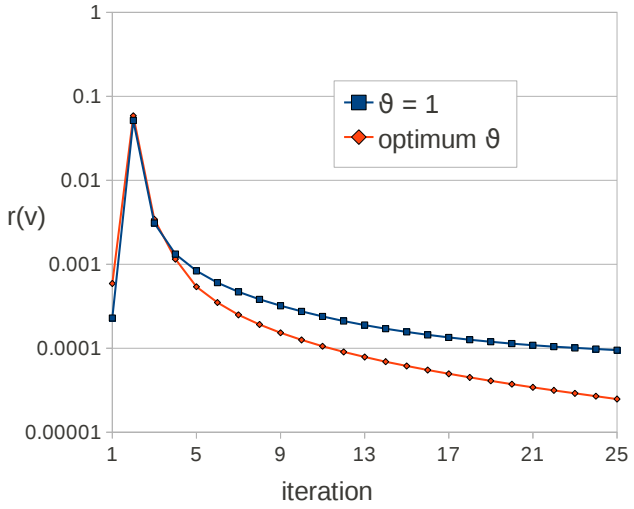

Figure 5: 2D water sloshing. Convergence of the velocities at t=1.75s for θ=1 and θ=0.0053.

In Fig. 7 the pressure solution at time t=1.75s obtained with θ=0.0053 is illustrated. It can be appreciated a remarkable enhancement with respect to the case of θ=1 (see Fig. 3). It is to be noted that the elements generated in the free surface region adjacent to the boundaries are due to the coarseness of the mesh and the remeshing criteria and not to the computation. For obtaining a better result, a smaller average mesh size or a refined mesh in the free surface region should be used.

As stated in Section 3, the convergence in the continuity equation affects the conservation of mass of the fluid. It has been just shown that the convergence of the pressure improves with a good prediction of θ. Consequently, also the mass conservation is better ensured using θ=0.0053 instead of θ=1.

In the graph of Fig. 8 the percentage of accumulated mass variation (in absolute value) versus time obtained with θ=1 and θ=0.0053 are compared. The better mass preservation of the solution with the smaller value of θ is remarkable.

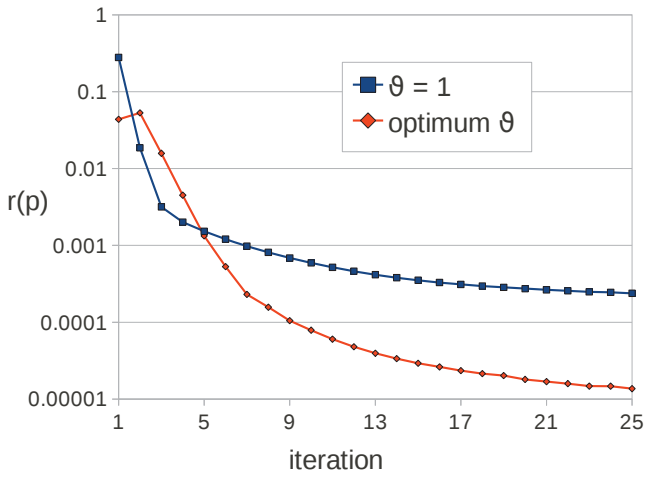

Figure 6: 2D water sloshing. Convergence of pressures at t=1.75s for θ=1 and θ=0.0053.

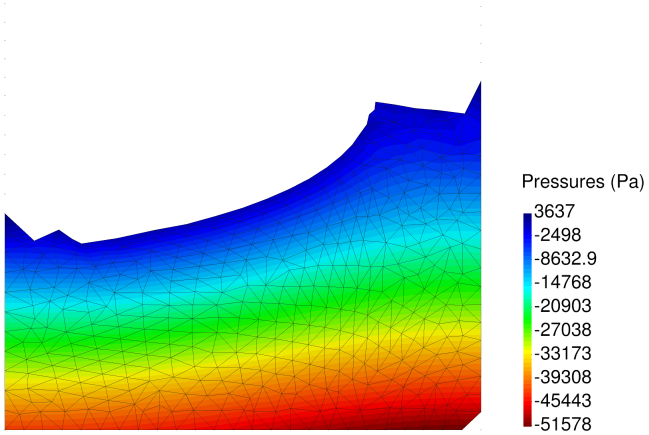

Figure 7: 2D water sloshing (θ=0.0053). Pressure contours at t=1.75s.

In the graph of Fig. 9 the accumulated mass variation obtained with θ=0.0053 is illustrated. After 20 seconds of simulation, the scheme with the reduced value of θ has an accumulated mass variation of 0.52% which correnspponds to a mean volume variation for each time step of $1.7 \cdot 10^{-3}$%. The solution with θ=0.0053 guarantees a better conservation of mass than the case with θ=1. This represents another evidence that the (quasi)-incompressibility constraint is not affected by the reduction of the bulk matrix in the iterative matrix for solving the momentum equations.

Variation on the mesh size

In order to verify the applicability of the method, the sloshing problem has been solved for Δt=$10^{-3}s$ and different mesh sizes. In particular, the following average mesh sizes have been

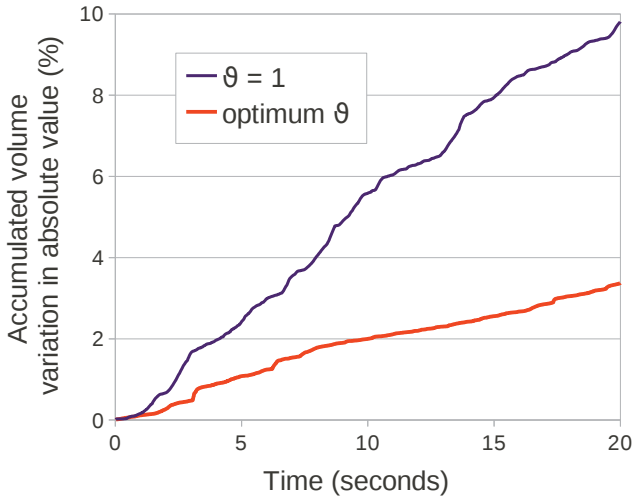

Figure 8: 2D water sloshing. Accumulated mass variation in absolute value along the duration of the analysis. Solution for θ=1 and θ=0.0053.

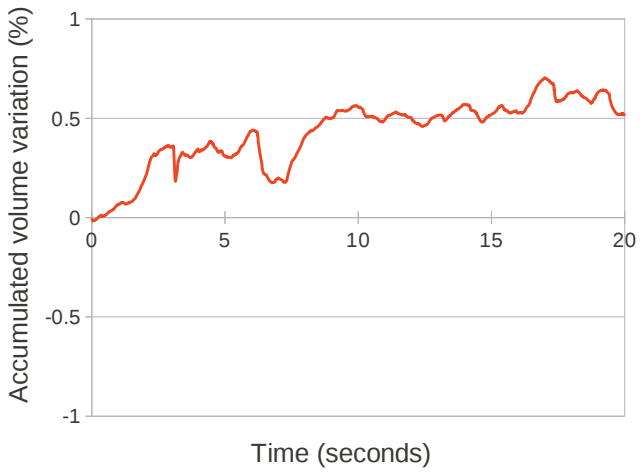

Figure 9: 2D water sloshing (θ=0.0053). Accumulated mass variation versus time.

chosen: h =0.1m, 0.15m, 0.2m, 0.3m and 0.4m.

The problem was solved setting θ=1 and computing *a priori* its reduced value using Eq.(22). The table of Fig. 10 collects all the data and the results. The number of iterations of the linear solver has been considered as a quality indicator of the analyses. As shown in the previous sections this value is related to the condition number of the iterative matrix.

The curves in Fig. 10 show, as it was foreseeable, that the reduced value of θ guarantees better results with respect to using $\theta = 1$. For all meshes, the number of iterations required by the linear solver to reach a converged solution is smaller. Furthermore, the results show that

the strategy is applicable to coarse and fine meshes.

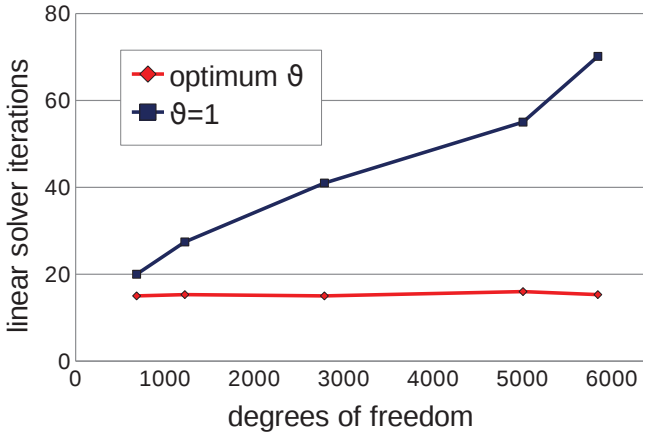

average mesh size	degrees of freedom (velocities)	number of iterations	
		θ=1	optimum θ
0.4	682	*20*	*15* (θ=0.535)
0.3	1220	*27*	*15* (θ=0.304)
0.2	2782	*41*	*15* (θ=0.136)
0.15	5002	*55*	*16* (θ=0.0801)
0.1	5840	*70*	*15* (θ=0.0361)

Figure 10: 2D water sloshing. Number of iterations of the linear solver for different numbers of velocity degrees of freedom. Results for θ=1 and the optimum value of θ.

Variations on the time step

The problem of Fig. 1 has been solved for different time steps: $0.0001s$, $0.0005s$, $0.001s$, $0.005s$, $0.01s$, $0.02s$. The mesh used has a mean size of $0.15m$. The numerical results obtained with the reduced value of θ and by setting θ=1 are compared. The table of Fig. 11 summarizes the problem data and the results. Once again, the iterations of the linear solver is the parameter chosen to indicate the quality of the analyses: the smaller this value is, the better conditioned the linear system is.

The graph of Fig. 11 shows that the accuracy of the method does not depend on the time step increments, when the suitable value for θ is used. For each value of Δt, the number of iterations is 16 and the condition number does not change. Furthermore, using the correct value of θ allows us to solve the problem for each time increment, while if θ is fixed to 1, the results are acceptable only until Δt=0.005s. For larger time steps the results for θ=1 are not accurate or the analyses do not even converge.

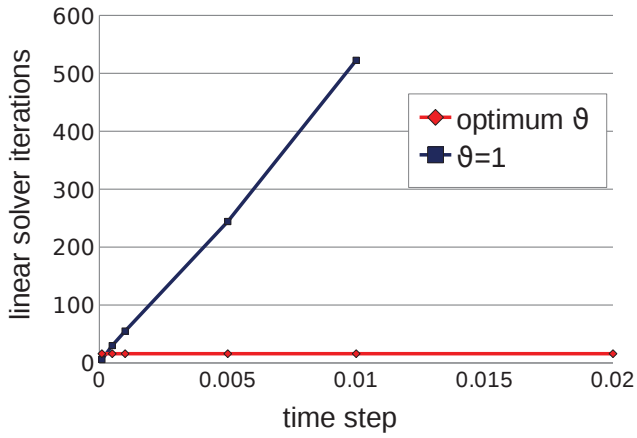

Δt (s)	number of iterations	
	θ=1	optimum θ
0.02	*failed*	*16* (θ=2.00 $\cdot 10^{-5}$)
0.01	*523*	*16* (θ=8.01 $\cdot 10^{-4}$)
0.005	*244*	*16* (θ=3.20 $\cdot 10^{-3}$)
0.001	*55*	*16* (θ=8.01 $\cdot 10^{-2}$)
0.0005	*30*	*16* (θ=3.89 $\cdot 10^{-1}$)
0.0001	*6*	*16* (θ=8.01)

Figure 11: 2D water sloshing. Number of iterations of the linear solver for different time step increments. Results for θ=1 and the optimum value of θ.

Mesh with a refined zone

As mentioned in the previous sections, the parameter θ has a square dependency on the mesh size (see Eq.(24)). For this reason, if the discretization is not uniform the global estimation of θ might not guarantee the well-conditioning of the linear system. In these cases, a local computation of θ is recommended. The sloshing problem is here solved again using the mesh shown in Fig. 12 and $\Delta t = 0.01s$. The spatial discretization has two different mean sizes: in the center h=0.1m while h=0.4m elsewhere. The problem is solved both for θ=1 and by computing its optimum value globally and locally. The mean number of iterations required by the linear solver to converge for each of these three options is 319, 21 and 17 respectively. Hence, the local approach guarantees the best result for this type of non-uniform meshes. In Fig. 13 the solution at time $t = 0.1s$ obtained with the local approach is illustrated.

Case with high viscosity

A high viscosity may improve the conditioning of the iteration matrix $\mathbf{H}_v$. In fact, the contribution of $\mathbf{K}$ has opposite sign versus that of $\mathbf{K}_v$. The sloshing problem is solved once

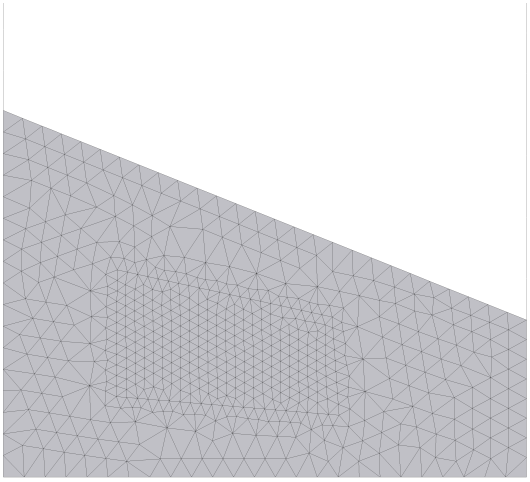

Figure 12: 2D water sloshing. Finite element mesh with a refined zone.

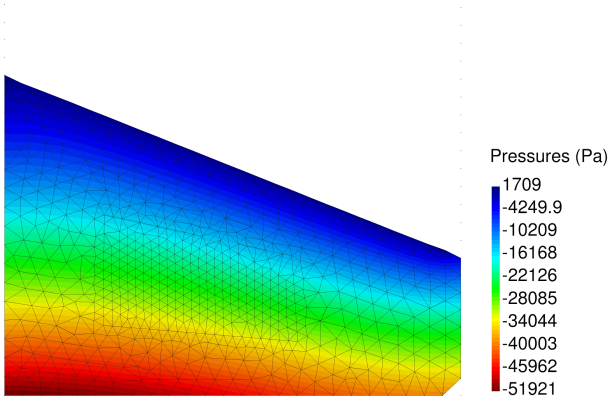

Figure 13: 2D sloshing with a refined zone. Solution at time $t = 0.1s$ obtained with the local approach.

more for a value of the dynamic viscosity μ=10^2Pa·s. The time increment is $\Delta t = 10^{-2}s$. In Fig. 14 the solutions at $t = 5.5s$ obtained by the two approaches are illustrated. The strategies converge to almost the same numerical value. This shows that the proposed method can also be used for highly viscous fluids. The condition number of $\mathbf{H}_v$ using θ =1 is C=2318 (note that, as expected, this value is lower than that obtained for the water sloshing case) while for $\theta = 5.35 \cdot 10^{-3}$ is C=23. In conclusion, for highly viscous fluids, the proposed method not only works but also leads to better conditioned tangent matrices than for θ =1.

6.2. Collapse of a water column on a rigid obstacle

In this section, the collapse of the water column induced by the instant removal of a vertical wall is studied. As for the previous example, the problem is first solved with a very coarse mesh. Then a comparison with the solution obtained for θ=1 is given. After that, the same problem

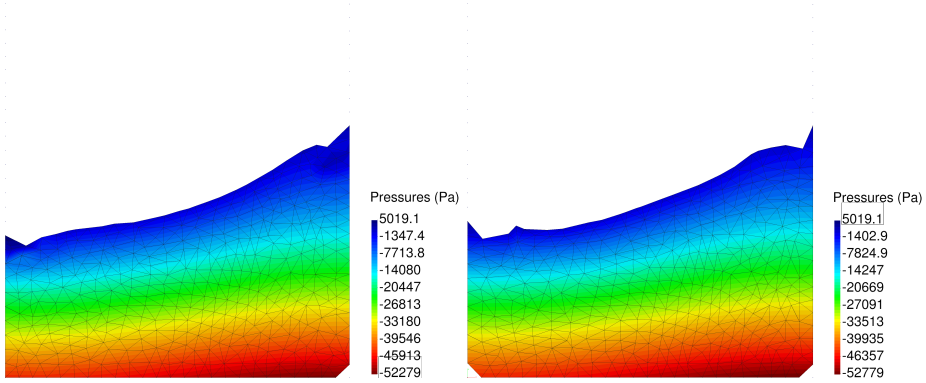

Figure 14: 2D high viscous fluid sloshing. Pressure contours at $t = 5.5s$. Left: numerical results for $\theta = 1$. Right: results for $\theta = 5.35 \cdot 10^{-3}$.

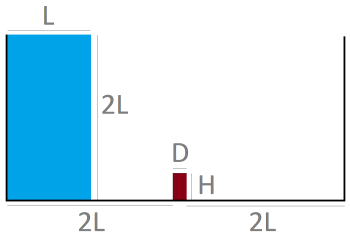

Figure 15: 2D dam break. Initial geometry.

L	0.146 m
H	0.048 m
D	0.024 m
viscosity	10^{-3} Pa·s
density	10^3 kg/m^3
bulk modulus	$2.15{\cdot}10^9$ Pa

Table II: 2D dam break. Problem data.

is solved for different mean sizes and different time step increments. The results obtained with the optimum value of θ are compared with the experimental results presented in [11]. The objective is to show that the reduction of the bulk modulus in the iteration matrix does not affect the numerical solution of this class of impact problems which can be solved also with a larger time step.

The initial geometry of the problem is illustrated in Fig. 15. In Table II all the data of the problem are collected.

The problem is first solved with a coarse discretization (mean element size h=0.0125m). The solutions obtained with the optimum value of θ and with θ=1 are compared in terms of the condition number of the iteration matrix and the number of iterations of the linear solver. For Δt=10^{-4}s, matrix $\mathbf{H}_v$ has condition numbers C=1028 and C=60, for θ=1 and θ=0.0535, respectively, which correspond to 1251 and 14 iterations of the linear solver, respectively. For the same discretization and a time increment of Δt=$10^{-3}s$, Eq.(22) yields a value of θ=0.000535. The condition number of $\mathbf{H}_v$ and the iterations of the linear solver are the same as using a time step increment ten times smaller. Conversely, for θ=1, the condition number grows to C=102090 and the iterative scheme does not converge.

Variation on the mesh size

The problem of Fig. 15 has been solved for $\Delta t{=}10^{-4}s$ using unstructured meshes with the following mean element sizes: $h{=}\ 0.004m$, $0.005m$, $00075m$, $0.01m$, $0.0125m$. The problem was solved both setting $\theta{=}1$ and computing *a priori* its optimum value via Eq.(22). As for the previous section, the number of iterations of the linear solver has been considered as the quality indicator of the analysis. In the table of Fig. 16 all the data and the results are collected.

Fig. 16 confirms that the efficiency of the method is not affected by the mesh size. In other words, the well-conditioning of the iterative matrix is guaranteed for coarse and fine meshes indifferently.

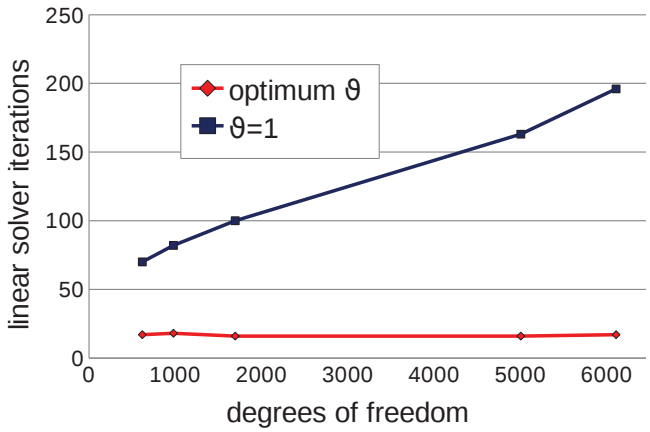

average mesh size	degrees of freedom (velocities)	number of iterations	
		$\theta{=}1$	optimum θ
0.0125	618	*70*	*17* ($\theta{=}0.0536$)
0.01	978	*82*	*18* ($\theta{=}0.0345$)
0.0075	1694	*100*	*16* ($\theta{=}0.0205$)
0.005	5002	*163*	*16* ($\theta{=}0.00868$)
0.004	6106	*196*	*17* ($\theta{=}0.00559$)

Figure 16: 2D dam break. Number of iterations of the linear solver for different numbers of velocity degrees of freedom. Results for $\theta{=}1$ and the optimum value of θ.

Variations on the time step

The same problem was solved with different time steps: $\Delta t{=}0.00005s$, $0.0001s$, $0.0005s$, $0.001s$, $0.0025s$. The mesh used has a mean size of $h{=}0.005m$. Table 17 collects the problem data and the resulting number of iterations for all the analyses solved with $\theta{=}1$ and with the optimum value of θ.

Fig. 17 confirms the conclusions of the previous section. The strategy is not affected by the time step and, contrary to the case with $\theta{=}1$, it does not impose limitations to the range of

time step increments for solving the problem. For example, for the present problem, the time step increment is constrained by the geometry and the dynamics of the problem only. In other words, the maximum time step increment is the one that guarantees that the fluid particles do not cross the boundaries. For the present problem and the chosen mesh, the maximum time step increment was Δt=2.5 $\cdot$ 10^{-3}s.

In Fig. 18 the pressure field and the comparison with experimental results [11] at $t = 0.1s$, $t = 0.2s$ and $t = 0.3s$ are shown. Very good agreement is obtained.

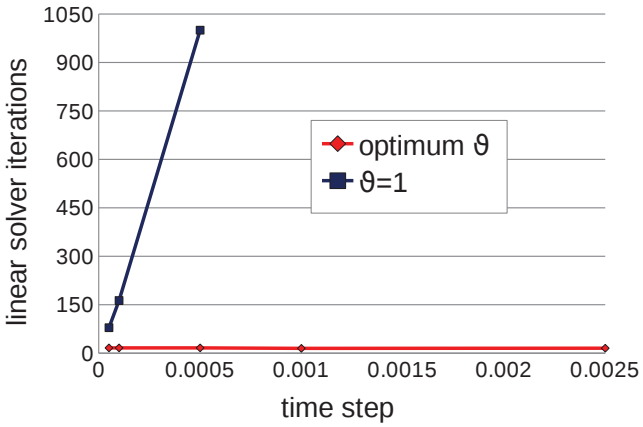

Δt (s)	numer of iterations	
	θ=1	optimum θ
$2.5 \cdot 10^{-3}$	*failed*	*15* (θ=1.39 $\cdot 10^{-5}$)
$1.0 \cdot 10^{-3}$	*failed*	*15* (θ=8.68 $\cdot 10^{-5}$)
$5.0 \cdot 10^{-4}$	*1000*	*16* (θ=3.47 $\cdot 10^{-4}$)
$1.0 \cdot 10^{-4}$	*163*	*16* (θ=8.68 $\cdot 10^{-3}$)
$5.0 \cdot 10^{-5}$	*79*	*16* (θ=3.47 $\cdot 10^{-2}$)

Figure 17: 2D dam break. Number of iterations of the linear solver for different time steps. Results for θ=1 and the optimum value of θ.

7. Conclusions

In this work, an analysis of the effects of the physical bulk modulus on the iteration matrix of a partitioned Lagrangian finite element scheme for analysis of quasi-incompressible fluids has been presented. It has been shown that the resulting linear system can be ill-conditioned for certain time step increments. It has been shown that the reason of this is the different order of magnitude of the contributions of the bulk and mass matrices in the solution system. Typically, the bulk matrix terms are larger than the mass ones. A consequence of the ill-conditioning

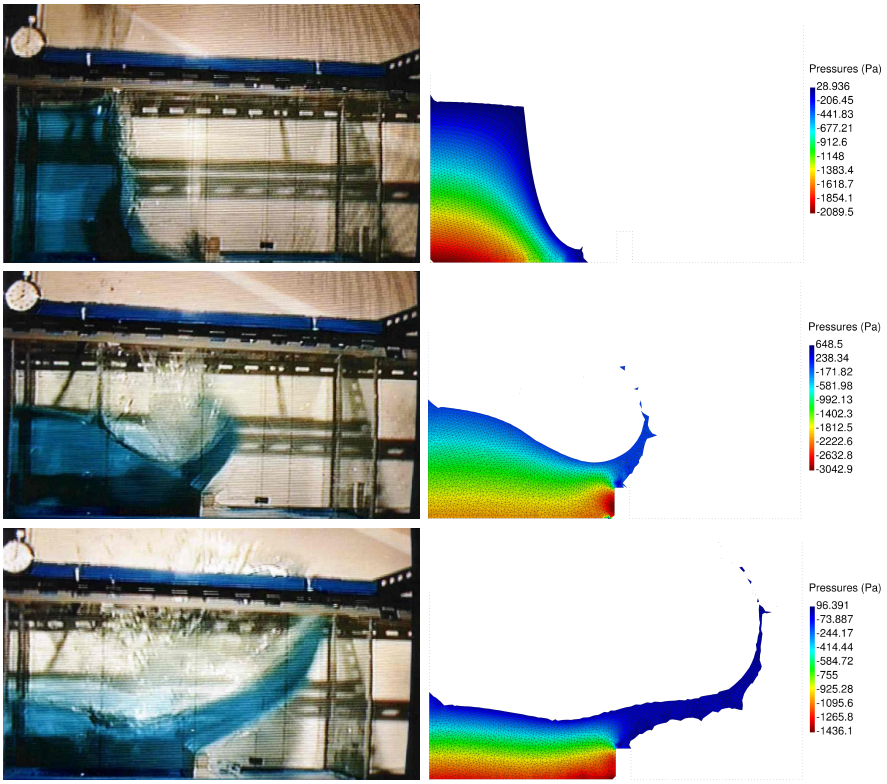

Figure 18: 2D dam break. Pressure contours and comparison with experimental results/left [11] at $t = 0.1s$, $t = 0.2s$ and $t = 0.3s$. Numerical results obtained with $\Delta t = 0.0025s$ and $\theta = 1.39 \cdot 10^{-5}$.

of the algebraic equations is that the convergence of both the linear iterative solver and the iterative loop is deteriorated.

A general, efficient and easy to implement strategy to overcome these problems has been proposed. The technique is based on using a pseudo bulk modulus $\kappa_p = \theta\kappa$ where $0 < \theta < 1$ in matrix $\mathbf{K}_v$ in order to improve the conditioning of the global iteration matrix $\mathbf{H}_v$. An expression for computing the optimum value of the reduction parameter θ has been given. The optimum value of θ can be computed locally or globally, and at each time step or only at the first solution step. Depending on the problem, one of these alternatives can be preferable. The parameter θ has the function to scale the bulk matrix terms in the iteration matrix so that they have the same order of magnitude than the mass matrix ones.

Numerical examples have shown that the proposed technique improves the stability of the pressure field, the convergence rate of the iterative solution and also the computational speed of the analysis of the iterative system. It has also been illustrated that the strategy is not affected by changes in the time step and the mesh. Furthermore, it has been shown that the method has also advantages for viscous fluids and locally refined meshes. For the latter case,

a local computation of the parameter θ is recommended.

Finally, it has been shown that it is possible to simulate impacts of fluids with very reduced values of θ without affecting the actual compressibility of the fluid.

Acknowledgements

This research was supported by Advanced Grant project SAFECON of the European Research Council.

References

[1] K.J. Bathe. *Finite Element Procedures.* Prentice-Hall, New Jersey, 1996.

[2] M. Benzi, G.H. Golub and J. Liesen. Numerical solution of saddle point problems. *Acta Numerica*, 14:1–137, 2005.

[3] M. Benzi, M.A. Olshanskii and Z. Wang. Modified augmented Lagrangian preconditions for the incompressible Navier-Stokes equations. *International Journal for Numerical Methods in Fluids*, 66:486–508, 2011.

[4] D. Bresch, E.D. Fernández-Nieto, I.R. Ionescu and P. Vigneaux. Augmented Lagrangian method and compressible visco-plastic flow. Applications to shallow dense avalanches. *New Directions in Mathematical Fluid Mechanics. The Alexander V. Kazhikhov Memorial Volume. In the Series of Book on Advances in Mathematical Fluid Mechanics. A.V. Fursikov, G.P. Galdi and V.V. Pukhnachev (Eds.)*, Birkhäuser Verlag Basel, Switzerland, 57–89, 2010.

[5] F. Brezzi. On the existence, uniqueness and approximation of saddle-point problems arising from lagrange multipliers. *Revue française d'automatique, informatique, recherche opérationnelle. Série rouge. Analyse numérique*, 8(R-2):129–151, November 1974.

[6] J.M. Carbonell, E. Oñate, and B. Suarez. Modeling of ground excavation with the particle finite-element method. *Journal of Engineering Mechanics*, 136:455–463, 2010.

[7] A.J. Chorin. A Numerical Method for Solving Incompressible Viscous Flow Problems. *Journal of Computational Physics*, 135:118–125,1997.

[8] J. Donea and A. Huerta. *Finite Element Methods for Flow Problems.* Wiley, 2003.

[9] H.C. Elman, D.J. Silvester and A.J. Wathen. *Finite element and fast iterative solvers with applications in incompressible fluid dynamics.* Oxford Series in Numerical Mathematics and Scientific Computation. Oxford University Press, Oxford, 2005.

[10] M. Fortin and R. Glowinski. Augmented Lagrangian: application to the numerical solution of boundary value problems. North-Holland, Amsterdam, 1983.

[11] D.M. Greaves. Simulation of viscous water column collapse using adapting hierarchical grids. *International Journal of Numerical Methods in Engineering*, 50:693–711, 2006.

[12] B. Hubner, E. Walhorn, and D.Dinkler. A monolithic approach to fluid-structure interaction using space-time finite elements. *Computer Methods in Applied Mechanics and Engineering*, 193:2087–2104, 2004.

[13] S.R. Idelshon, J. Marti, A. Limache, and E. Oñate. Unified lagrangian formulation for elastic solids and incompressible fluids: Applications to fluid-structure interaction problems via the PFEM. *Computer Methods In Applied Mechanics And Engineering*, 197:1762–1776, February 2008.

[14] S.R. Idelsohn, E. Oñate, and F. Del Pin. The particle finite element method: a powerful tool to solve incompressible flows with free-surfaces and breaking waves. *International Journal for Numerical Methods in Engineering*, 61:964–989, 2004.

[15] A. Larese, R. Rossi, E. Oñate, and S.R. Idelsohn. Validation of the particle finite element method (PFEM) for simulation of free surface flows. *International Journal for Computer-Aided Engineering and Software*, 25:385–425, 2008.

[16] E. Oñate. Derivation of stabilized equations for advective-diffusive transport and fluid flow problems. *Computer Methods in Applied Mechanics and Engineering.* 151:233–267, 1998.

[17] E. Oñate. A stabilized finite element method for incompressible viscous flows using a finite increment calculus formulation. *Computer Methods in Applied Mechanics and Engineering* 182(1–2):355–370, 2000.

[18] E. Oñate and J.M. Carbonell. Updated lagrangian finite element formulation for quasi and fully incompressible fluids. *Accepted in Computational Mechanics*, 2014.

[19] E. Oñate, A. Franci, and J.M. Carbonell. Lagrangian formulation for finite element analysis of quasi-incompressible fluids with reduced mass losses. *International Journal for Numerical Methods in Fluids*, 74:699–731, 2014.

[20] E. Oñate, A. Franci, and J.M. Carbonell. A particle finite element method for analysis of industrial forming processes. *Computational Mechanics*, 54:85–107, 2014.

[21] E. Oñate, A. Franci, and J.M. Carbonell. A particle finite element method (PFEM) for coupled thermal analysis of quasi and fully incompressible flows and fluid-structure interaction problems. In *Numerical Simulations of Coupled Problems in Engineering*, S.R. Idelsohn (Ed.), Vol. 33, pp 129–156, Series in Computational Methods in Applied Sciences, Springer 2014.

[22] E. Oñate, S.R. Idelsohn, F. Del Pin, and R. Aubry. The particle finite element method. An overview. *International Journal for Computational Methods*, 1:267–307, 2004.

[23] E. Oñate. Possibilities of finite calculus in computational mechanics. *International Journal for Numerical Methods in Engineering* 60(1):255–281, 2004.

[24] E. Oñate, P. Nadukandi, S.R. Idelsohn, J. García, and C. Felippa. A family of residual-based stabilized finite element methods for stokes flows. *International Journal for Numerical Methods in Fluids*, 65(1-3):106–134, 2011.

[25] E. Oñate, A. Valls, and J.García. Computation of turbulent flows using a finite calculus-finite element formulation. *International Journal of Numerical Methods in Engineering*, 54:609–637, 2007.

[26] P. Ryzhakov. *Doctoral thesis: Lagrangian FE Methods for Coupled Problems in Fluid Mechanics*. Universitat Politècnica de Catalunya, Barcelona, Spain, 2010.

[27] P. Ryzhakov, J. Cotela, R. Rossi, and E. Oñate. A two-step monolithic method for the efficient simulation of incompressible flows. *International Journal for Numerical Methods in Fluids*,74:919–934,2014.

[28] P. Ryzhakov, E. Oñate, and S.R. Idelsohn. Improving mass conservation in simulation of incompressible flows. *International Journal of Numerical Methods in Engineering*, 90:1435–1451, 2012.

[29] P. Ryzhakov, R. Rossi, S.R. Idelsohn, and E. Oñate. A monolithic lagrangian approach for fluid-structure interaction problems. *Computational Mechanics*, 46:883–899, 2010.

[30] E. Turkel. Preconditioned Methods for Solving the Incompressible and Low Speed Compressible Equations. *Journal of Computational Physics*, 72:277–298, 1987.

[31] G. Vinay, A. Wachs and J.F. Agassant. Numerical simulation of weakly compressible Bingham flows: The restart of pipeline flows of waxy crude oil. *Journal of Non-Newtonian Fluids Mechanics*, 136(2–3):93–105, 2006.

[32] S. Vincent, Al Sarthou, J.P. Caltagirone, F. Sonilhac, P. Février, C. Mignot and G. Pianet. Augmented Lagrangian and penalty methods for the simulation of two-phase flows interacting with moving solids. Application to hydroplanning flows interacting real tire tread patterns. *Journal of Computational Physics*, 203(4):956–983, 2013.

[33] O.C. Zienkiewicz and R.L. Taylor. *The Finite Element Method. Its Basis and Fundamentals. (6th Ed.)*. Elsevier Butterworth-Heinemann, Oxford, 2005.

[34] O.C. Zienkiewicz, R.L. Taylor, and P. Nithiarasu. *The Finite Element Method for Fluid Dynamics,Volume 3 (6th Ed.)*. Elsiever, Oxford, 2005.